On the diagnosis of radiative feedback in the presence of unknown radiative forcing

Roy W. Spencer[1] and William D. Braswell[1]

Received 12 October 2009; revised 29 March 2010; accepted 12 April 2010; published 24 August 2010.

[1] The impact of time-varying radiative forcing on the diagnosis of radiative feedback from satellite observations of the Earth is explored. Phase space plots of variations in global average temperature versus radiative flux reveal linear striations and spiral patterns in both satellite measurements and in output from coupled climate models. A simple forcing-feedback model is used to demonstrate that the linear striations represent radiative feedback upon nonradiatively forced temperature variations, while the spiral patterns are the result of time-varying radiative forcing generated internal to the climate system. Only in the idealized special case of instantaneous and then constant radiative forcing, a situation that probably never occurs either naturally or anthropogenically, can feedback be observed in the presence of unknown radiative forcing. This is true whether the unknown radiative forcing is generated internal or external to the climate system. In the general case, a mixture of both unknown radiative and nonradiative forcings can be expected, and the challenge for feedback diagnosis is to extract the signal of feedback upon nonradiatively forced temperature change in the presence of the noise generated by unknown time-varying radiative forcing. These results underscore the need for more accurate methods of diagnosing feedback from satellite data and for quantitatively relating those feedbacks to long-term climate sensitivity.

Citation: Spencer, R. W., and W. D. Braswell (2010), On the diagnosis of radiative feedback in the presence of unknown radiative forcing, *J. Geophys. Res.*, *115*, D16109, doi:10.1029/2009JD013371.

1. Introduction and Background

[2] The sensitivity of the climate system to long-term radiative forcing from anthropogenic greenhouse gas emissions remains the greatest source of uncertainty in projections of future climate change [*Intergovernmental Panel on Climate Change* (*IPCC*), 2007]. Unfortunately, the diagnosis of the feedbacks that determine climate sensitivity from observational data has been hampered by uncertain and conflicting results. In the face of this uncertainty, investigators have turned to other methods of estimating climate sensitivity, such as temperature proxy responses to presumed forcings involved in ancient climate change events or reliance on climate models, which are adjusted to mimic other observed features of the present day climate system. *Knutti and Hegerl* [2008] provide a review of numerous estimates of climate sensitivity obtained by a variety of methods.

[3] While others have concluded that feedbacks are difficult to accurately diagnose [e.g., *Aires and Rossow*, 2003; *Stephens*, 2005], there has been little investigation into the specific reasons why this would be the case. The importance of the climate sensitivity issue demands a more thorough understanding of the processes which influence variations in the top-of-atmosphere (TOA) radiative budget, including the conditions under which accurate or inaccurate feedback diagnoses might be expected.

[4] The impetus for this study is the existence of peculiarities found during our analysis of satellite observations of thermally emitted longwave (LW) and reflected solar shortwave (SW) radiative flux and temperature variations. This led us to reexamine the established method of diagnosing feedbacks wherein the slope of a linear regression fit to the covariations between globally averaged TOA radiative flux variations and temperature variations is measured.

[5] We will argue that the largest source of error in feedback diagnosis is the presence of time-varying radiative forcing generated internal to the climate system, which then contaminates the radiative feedback signal. Removal of known radiative forcings from the data in order to diagnose radiative feedback has been demonstrated by *Forster and Taylor* [2006, hereafter FT06] in their diagnosis of the long-term feedbacks operating in the IPCC AR4 coupled climate models and by *Forster and Gregory* [2006, hereafter FG06] in their satellite diagnosis of LW and SW feedbacks in response to the aerosol radiative forcing after the 1991 eruption of Mt. Pinatubo. But what has not been addressed in any systematic way is the impact of unknown radiative forcings on the diagnosis of feedback.

[6] We will show that the signature of internally generated radiative forcing, such as nonfeedback variations in cloud

[1]Earth System Science Center, University of Alabama in Huntsville, Huntsville, Alabama, USA.

0148-0227/10/2009JD013371

cover, is ubiquitous in both satellite measurements and in coupled atmosphere-ocean general circulation models (AOGCMs). While some investigators have called this "unforced internal variability" [e.g., *Wong et al.*, 2006], we will argue that it is more consistent and less confusing within the forcing-feedback paradigm of climate change to call such variations internal radiative forcing.

2. A Simple Model of Forcing and Feedback

[7] Considerable insight into the issues impacting the diagnosis of feedback can be gained with the simple time-dependent forcing-feedback model represented by

$$C_p[dT_{sfc}/dt] = F(t) - \lambda_{net} T_{sfc}(t), \quad (1)$$

where T_{sfc} is the global average surface temperature deviation away from an equilibrium state of energy balance, C_p is the bulk heat capacity of the system, F represents one or more heat flux forcings (energy imbalances) causing temperature departures from equilibrium, and λ_{net} is the net radiative feedback parameter, the reciprocal of which is the climate sensitivity parameter of the simple modeled system. It is important to recognize that, while feedback in this simple model is explicitly specified through the $\lambda_{net} T_{sfc}$ term, the feedbacks in AOGCMs are not specified but are instead the net result of how the various physical processes in those models combine to lead to temperature-dependent changes in the TOA radiative budget.

[8] The feedback parameter λ_{net} is the sum of all reflected SW and thermally emitted LW feedbacks,

$$\lambda_{net} = \lambda_{SW} + \lambda_{LW}, \quad (2)$$

the reciprocal of which is the climate sensitivity parameter. The longwave feedback parameter λ_{LW} also includes the "Planck" (or "Stefan-Boltzman") direct response of the outgoing longwave flux to temperature change, amounting to about 3.3 W m^{-2} K^{-1} at the average effective radiating temperature of the Earth, 255 K. Negative SW or LW feedbacks add positively to the radiative loss of the system as temperature increases, pushing the feedback parameter to values greater than 3.3 W m^{-2} K^{-1}. Positive feedbacks reduce the radiative loss by the system in response to a temperature rise, leading to λ_{net} values less than 3.3 W m^{-2} K^{-1}.

[9] Note that if positive feedbacks (which contribute negatively to the feedback parameter) were to more than cancel out the Planck response of 3.3 W m^{-2} K^{-1}, then the feedback parameter becomes negative and the system represented by equation (1) is potentially unstable to perturbations. As we will see, negative feedback parameters can be erroneously diagnosed if sufficient time-varying radiative forcing is present.

[10] Most of the AR4 models have net feedback parameters between 1 and 2 W m^{-2} K^{-1} (FT06). While this is a fairly narrow range, it represents a wide range of equilibrium climate sensitivities: 1.9°C–3.8°C of warming for a doubling of atmospheric carbon dioxide ($2\times CO_2$) assumed here to cause a LW forcing of 3.8 W m^{-2}. This is because of the reciprocal relationship of climate sensitivity to feedback, so that feedback values sufficiently close to zero can correspond to a wide range of high climate sensitivities [e.g., *Lindzen and Choi*, 2009].

[11] There are different ways in which equation (1) can be used to diagnose feedback. For example, since individual radiative forcings cause a temperature response that decays exponentially with time, the autocorrelation structure exhibited by the time series of global average temperature can be analyzed to estimate feedback in the system. This method has yielded a variety of results [*Gregory et al.*, 2002; *Schwartz*, 2007; *Knutti et al.*, 2008; *Schwartz*, 2008; *Foster et al.*, 2008; *Scafetta*, 2008], but its utility is limited by sensitivity to the assumed heat capacity of the system [e.g., *Kirk-Davidoff*, 2009].

[12] The simpler method we analyze here is to regress the TOA radiative variations against the temperature variations. If the radiative variations are due only to feedback (a critical requirement which we will show is, in general, not met), then regression of the radiative feedback term $\lambda_{net} T_{sfc}$ against T_{sfc} will yield λ_{net}, no matter what the system heat capacity is. Note that the question of whether any feedback diagnosed from short-term climate variability is an indicator of long-term climate sensitivity is a separate problem.

[13] The central issue we will examine is that satellite measurements of variations in radiative flux contain a mixture of forcing and feedback and the presence of one will affect the identification and estimation of the other. Our specific interest is a better understanding of the impact that unknown levels of time-varying radiative forcing have on feedback diagnosis and what that might mean for the estimation of climate sensitivity.

3. Satellite Data Analysis

[14] Our first satellite data analysis is based upon Terra CERES [*Wielicki et al.*, 1996] Edition 2 ERBE-like ES4 LW and SW daily average radiative fluxes, with the REV1 SW drift corrections applied. We computed monthly global anomalies in both TOA LW and reflected SW fluxes from CERES and compared them to anomalies in either deep-layer midtropospheric temperature estimates (T_{MT}) [*Christy et al.*, 2003] or to HadCRUT3 surface temperature (T_{sfc}) anomalies [*Brohan et al.*, 2006]. We compute anomalies as deviations from the average annual cycles in these two data sets over the 9 year CERES period of record extending from March 2000 through December 2008.

[15] Globally averaged anomalies in CERES net (LW + SW) fluxes are plotted against midtroposphere temperature estimates in Figures 1a, 1c, and 1e and against surface temperature anomalies in Figures 1b, 1d, and 1f. The sets of three frames are for 1, 3, and 7 month averaging times, respectively. As can be seen, there is considerable scatter in the relationships no matter whether tropospheric or surface temperatures are used and at all three averaging times. This is consistent with low correlations found in the Earth Radiation Budget Experiment (ERBE) regression analysis of FG06, whose regressions averaged only 15% explained variance. The regression slopes in Figure 1 range from near-zero to 2.5 W m^{-2} K^{-1}, depending upon the averaging period, and whether surface or tropospheric temperatures are used, which illustrates why satellite diagnoses of feedback have remained so uncertain. Since all explained variances are rather low, there is great uncertainty in the value of each slope.

[16] At high time resolution, we even find some evidence of a negative regression slope when referenced to surface tem-

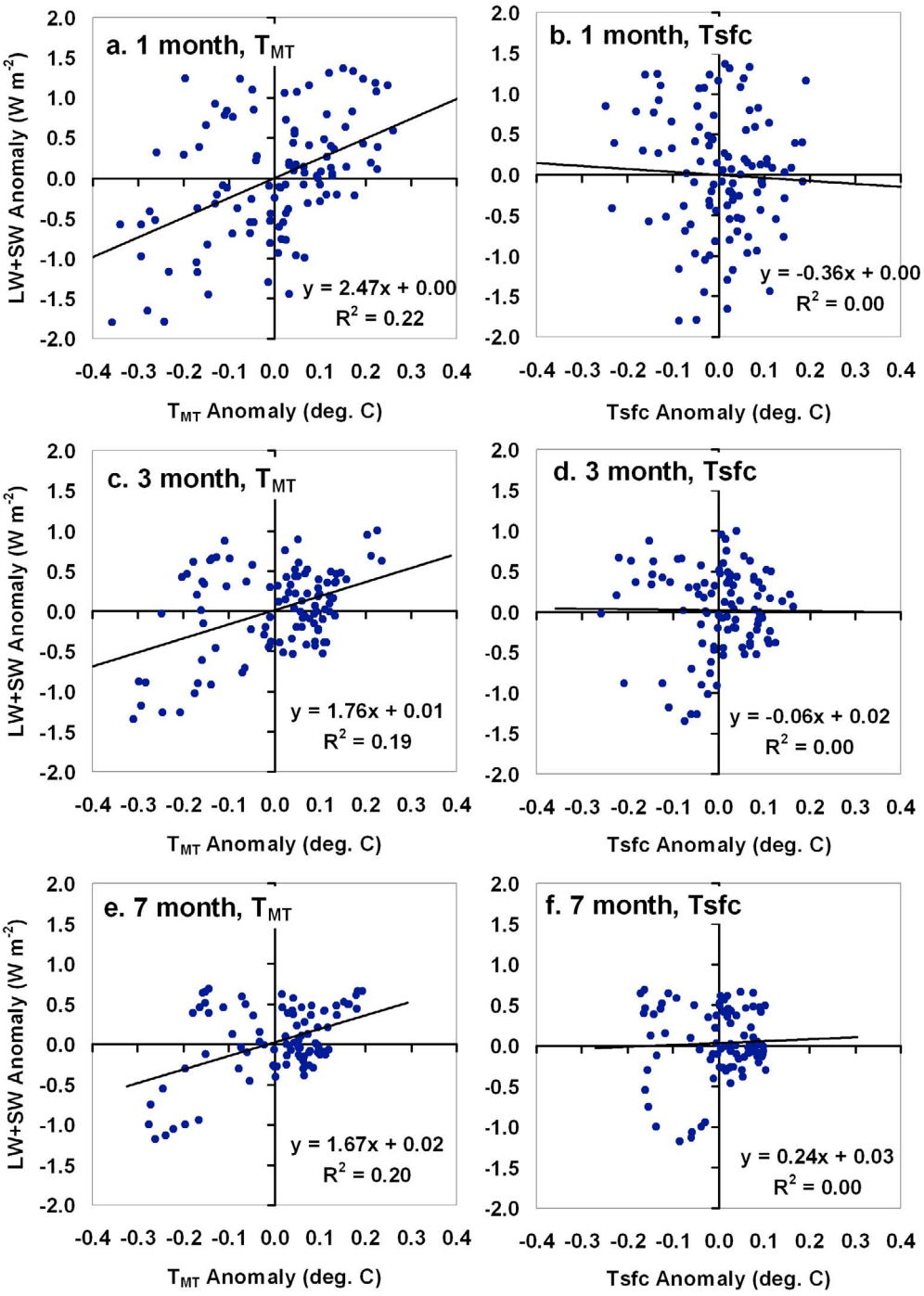

Figure 1. Global average Terra CERES net (LW + SW) radiative flux anomalies (a, c, and e) versus UAH midtropospheric temperature (T_{MT}) anomalies and (b, d, and f) versus HadCRUT3 surface temperature (T_{sfc}) anomalies at the indicated averaging times of 1, 3, and 7 months during the period March 2000 through December 2008.

perature. This cannot represent the real sensitivity of the climate system since, as mentioned previously, the system would be unstable to perturbations. This behavior becomes more apparent when the data averaging time is reduced to less than monthly. For instance, if we restrict the analysis to the global oceans (60°N–60°S latitude) where we have approximately daily, near-all-weather sea surface temperatures (SSTs) from the Advanced Microwave Scanning Radiometer (AMSR-E) flying on NASA's Aqua spacecraft, we can approach daily time resolution. We computed daily radiative flux anomalies in the AMSR-E SSTs available from remote sensing systems and in the radiative fluxes measured by the

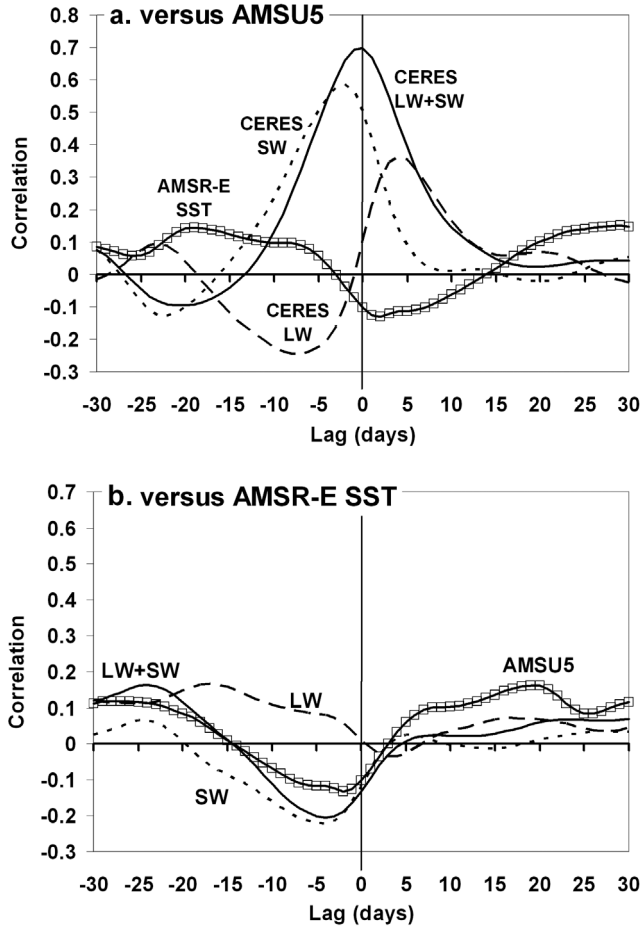

Figure 2. Lag correlation plots of daily global ocean-averaged anomalies in LW, SW, and net (LW + SW) radiative flux as measured by CERES (a) versus tropospheric temperature from AMSU channel 5 and (b) versus sea surface temperature.

CERES flying on the Aqua spacecraft. The midtropospheric temperature anomalies now come from channel 5 of the Advanced Microwave Sounding Unit (AMSU-A) flying on the NOAA-15 satellite since the T_{MT} products (which are also based upon AMSU channel 5) do not include ocean-only averages at daily time resolution. In Figure 2a, we see that there is a high correlation (r = 0.70) at zero days time lag between tropospheric temperature and net (LW + SW) radiative flux even though the temperature and radiative flux measurements come from instruments on different spacecraft. But the radiative flux correlations with SST, in stark contrast, are weakly negative (Figure 2b) despite the two measurements coming from the same spacecraft.

[17] The fact that radiative flux variations are much more strongly correlated with tropospheric temperature than surface temperature suggests a stronger feedback relationship at the shorter, intraseasonal time scales. Later we will see that this difference in behaviors at high time resolution is related to a type of forcing in the climate system that actually facilitates the identification of radiative feedback.

[18] Of course, as the time scale is increased, the coupling between surface and tropospheric temperature variations can be expected to be much stronger. Table 1 provides some regression statistics between these two temperature measures for both standard least squares regression (the dependent variable T_{MT} estimated from the independent T_{sfc}) and a two-way regression coefficient estimate based upon the geometric mean of two slopes where one of the regressions has the two variables interchanged. The statistics in Table 1 reveal that global average surface and tropospheric temperature anomalies do indeed become better correlated as the averaging time is lengthened, reaching 75% explained variance for yearly global averages. The midtropospheric temperature anomalies are somewhat magnified compared to the surface temperature anomalies, a fact which must be kept in mind if comparing feedback parameters computed relative to the different temperature measures.

[19] We find that considerable physical insight into the covariations between radiative flux and temperature can be gained through phase space plotting of the data. Using the 1 month comparisons between CERES radiative fluxes and T_{MT} in Figure 1a as an example, if we connect the data points in time sequence (Figure 3a), we can visualize the time evolution or "trajectory" of the system. In this case, we see evidence of linear striations having a steeper slope than a linear regression fit using all of the data together. Those striations are approximately parallel to the dashed line, which is drawn to have a slope of 6.2 W m^{-2} K^{-1}. This value is the average slope of all of the month-to-month line segments in Figure 3a. These striations are significantly different from a similar plot of two time series of random numbers, shown in Figure 3b, suggesting that the striations are due to some underlying physical process.

[20] A second behavior we find in phase space plots of the data is spiral or looping patterns, especially when running averages are plotted. While this would be expected to some extent simply from the averaging process alone, some of the features are quite striking, as shown in Figure 4. In Figure 4a, there is a large looping structure in Terra CERES data that corresponds to the strong global cooling event of late 2007 and early 2008. A similar loop is seen in Figure 4b based upon recalibrated ERBE data [*Wong et al.*, 2006] associated with the cooling that occurred after the June 1991 eruption of Mt. Pinatubo. Because of orbital limitations of the Earth Radiation Budget Satellite (ERBS), the ERBE anomalies

Table 1. Regression Relationships Between Global Average Surface Temperature Anomalies and Midtropospheric Temperature Anomalies During March 2000 Through December 2008 at Various Data Averaging Intervals

Regression Slope Type	Monthly Slope (R2)	3 Months Slope (R2)	7 Months Slope (R2)	12 Months Slope (R2)
$\Delta T_{MT}/\Delta T_{sfc}$	0.89 (39%)	1.05 (54%)	1.17 (63%)	1.44 (75%)
Geometric mean	1.42	1.43	1.47	1.67

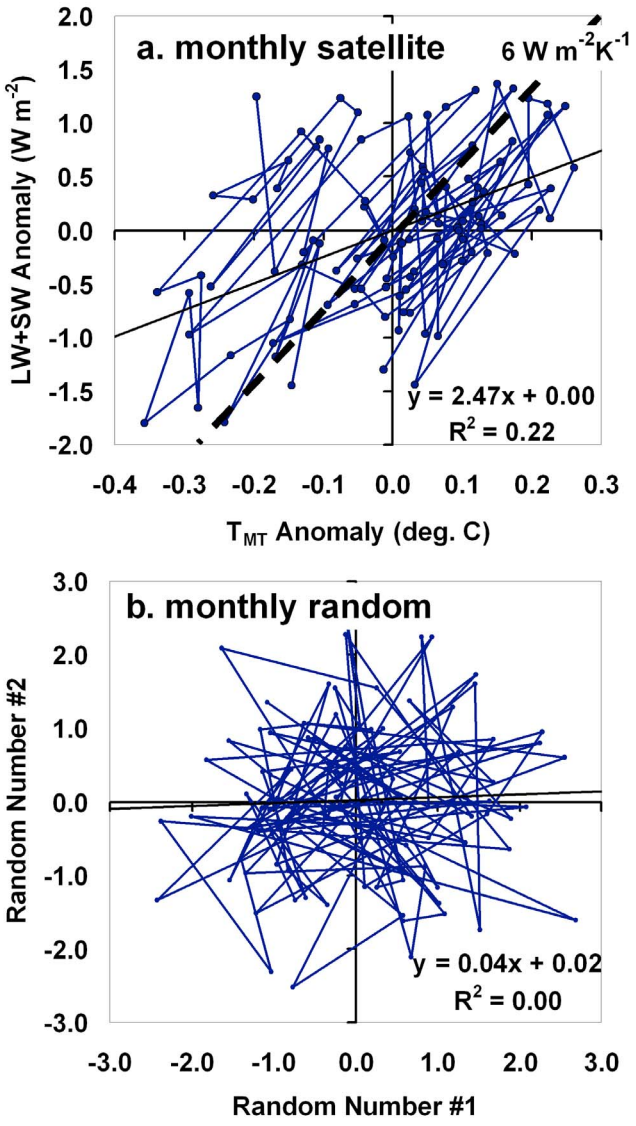

Figure 3. (a) As in Figure 1a, but a phase space plot of the data points connected in time sequence. The dashed line represents the average slope of all month-to-month line segments. (b) Phase space plot of two separate time series of normally distributed random numbers.

cover the latitude range of 60°N–60°S and must be averaged to five 72 day periods per year to prevent aliasing of the diurnal cycle into the anomalies.

4. Climate Simulations With the Simple Model

[21] All of the behaviors seen so far (very low correlations between temperature and radiative flux anomalies, substantially different regression slopes for radiative flux relative to tropospheric versus surface temperature, and linear striations or spirals in phase space plots of the data) can be explained based upon a few fairly simple, yet fundamental, processes that can be demonstrated with the simple forcing-feedback model represented by equation (1). We will begin with the familiar, but idealized, example of instantaneous radiative forcing, since it seems to have led to some misunderstanding regarding the diagnosis of feedback in the climate system. We will then add increasing levels of realism to the simple model.

4.1. Case 1: Classic Case of Instantaneous Radiative Forcing

[22] In the idealized case of instantaneous radiative forcing, the climate system is assumed to be in an initial state of radiative equilibrium at a constant average temperature, with the rate of absorption of SW energy by the Earth equaling the rate of emitted LW energy. Then the Earth's radiative balance is upset by the instantaneous introduction of a radiative forcing agent, for instance, a doubling of the carbon dioxide concentration of the atmosphere, which is then kept constant over time.

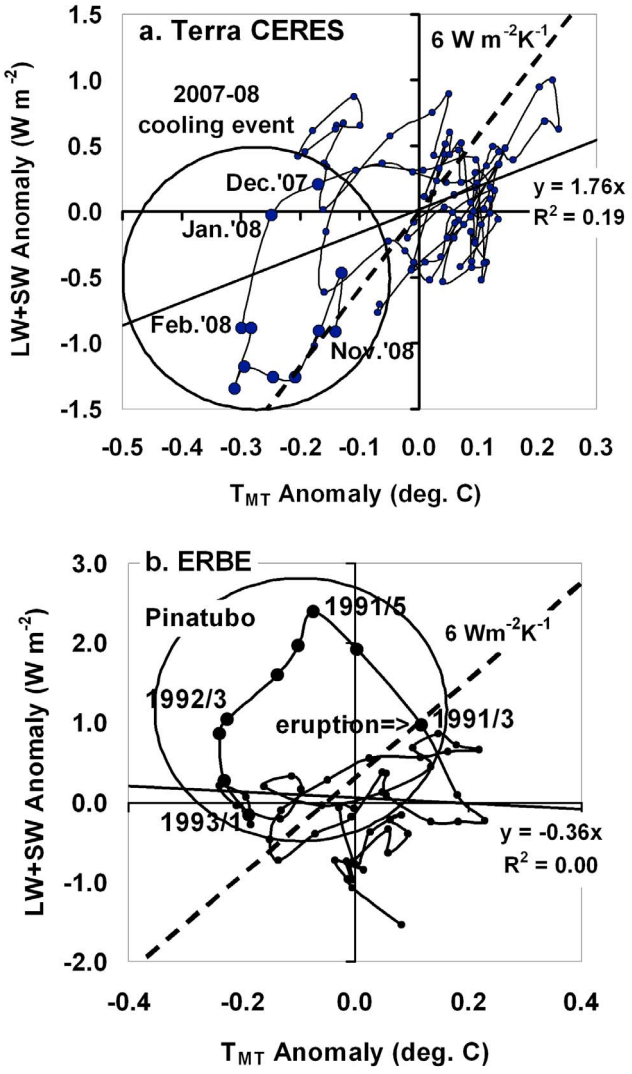

Figure 4. Net (LW + SW) radiative flux anomalies versus middle tropospheric temperature (T_{MT}) anomalies from (a) CERES during March 2000 through December 2008, 3 month anomalies plotted every month, and (b) ERBE during 1985 through 1999, 216 day anomalies plotted every 72 days. There are five 72 day periods in a calendar year, and the date labels shown in Figure 4b refer to which centered 72 day period the data point corresponds to.

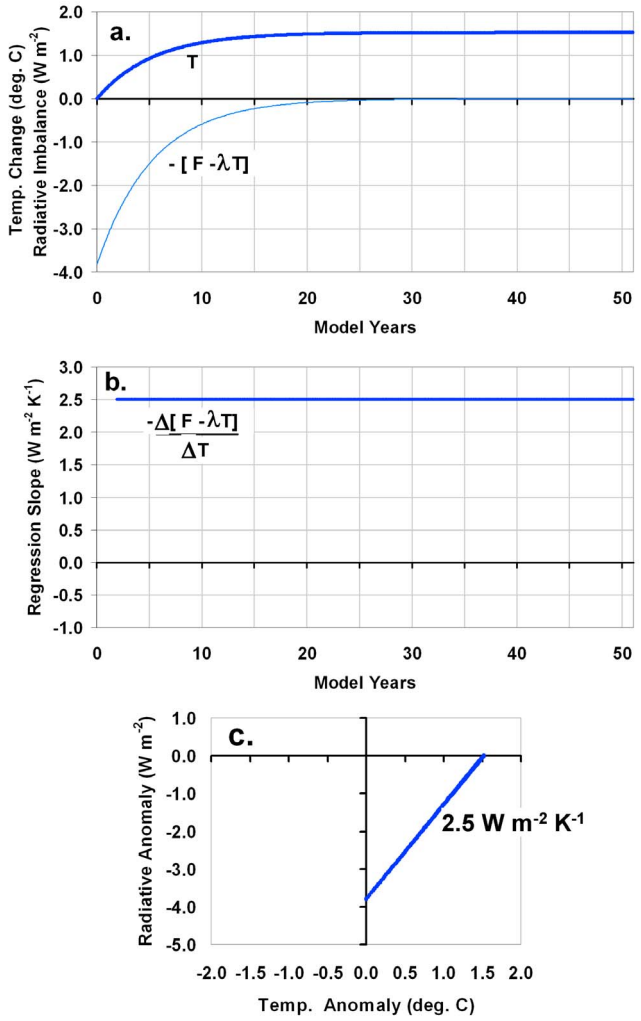

Figure 5. Output of a simple forcing-feedback model instantaneously forced with an energy imbalance of 3.8 W m^{-2}, displayed as (a) time series of the model temperature and total TOA radiative flux variations, (b) time series of regression slopes computed from the two time series in Figure 5a over the period of record up to that time, and (c) scatterplot of the temperature and radiative flux data against one another. A uniformly mixed (swamp) ocean 100 m deep and a feedback parameter of 2.5 W m^{-2} K^{-1} were assumed in this experiment.

[23] If we run a finite difference form of the model represented by equation (1) with a time step of 1 month, a heat capacity equivalent to a perfectly mixed (swamp) ocean layer depth of 100 m, a feedback parameter of 2.5 W m^{-2} K^{-1}, and an instantaneous forcing of 3.8 W m^{-2} representing $2\times CO_2$, then the resulting changes in temperature and radiative imbalance shown in Figure 5a result. This idealized case of constant radiative forcing has an analytical solution, with an exponentially decaying temperature response with time [e.g., *Gregory et al.*, 2004]. As mentioned previously, the exponential decay behavior is the basis of the feedback diagnosis method of *Schwartz* [2007] and others.

[24] If we plot the resulting temperature variations against the radiative flux variations (see Figure 5c), we find that the data fall neatly along a line, the slope of which exactly matches the feedback specified in the model simulation, 2.5 W m^{-2} K^{-1}. As discussed by *Gregory et al.* [2004] and as shown in Figure 5b, one need not wait for a new equilibrium state to be reached to diagnose the feedback (and thus the equilibrium climate sensitivity) in the case of instantaneous radiative forcing. This is because, in the absence of noise or time variations in feedbacks or system heat capacities, the initial changes in temperature and net radiative flux will immediately and precisely follow the feedback specified in the model run. Replacement of our assumed values for forcing, feedback, or heat capacity with other values (not shown) would reveal that the relationships shown in Figures 5b and 5c remain unchanged.

[25] But the only reason why feedback can be accurately diagnosed in this case is that all of the radiative variability is due to feedback, since the radiative forcing remains constant as the system relaxes to a new state of equilibrium. This fact raises a somewhat obscure point that is seldom if ever mentioned: the radiative forcing does not go away when energy balance is restored. The radiative forcing remains in the system, which is why the temperature response remains in the system. A new state of radiative balance is reached when the radiative feedback response to the warming exactly offsets the radiative forcing. While this distinction between radiative forcing and radiative imbalance is a subtle one, we will see that it permits a more consistent conceptual understanding of the relationships between forcing and feedback.

4.2. Case 2: Transient Radiative Forcing

[26] While the previous idealized case has been widely exploited both qualitatively and quantitatively, there is probably no real-world example where radiative forcing is instantaneously imposed and then remains constant. For instance, the carbon dioxide concentration of today's atmosphere was not instantaneously increased but has been slowly growing over time. This is why coupled climate models are now run with transient radiative forcing, often an assumed 1% annual growth rate in the carbon dioxide concentration of the model atmosphere. And while an explosive volcanic eruption might at first seem to be a good example of instantaneous radiative forcing, that forcing does not remain constant but diminishes over time.

[27] To demonstrate how feedback diagnosis is affected by transient radiative forcing, we again ran the same simple model, but with the radiative forcing increasing linearly with time at a rate of 0.4 W m^{-2} per decade, which approximates a doubling of the CO_2 concentration of the atmosphere over 100 years. The modeled radiative imbalance and temperature then evolve as is shown in Figure 6a. As can be seen, the model behavior is very different from the instantaneous radiative forcing case shown in Figure 5. Since the transient radiative forcing keeps increasing with time, so does the warming.

[28] But more significant to our goal of diagnosing feedbacks, Figures 6b and 6c reveal that a regression slope computed at any point in time in the model simulation will not only be different from the specified feedback of 2.5 W m^{-2} K^{-1}, it will always result in a negative regression slope. Upon some reflection, we realize that this must be the case since the radiative forcing accumulates faster than the radiative feedback can relieve the imbalance for any system with finite heat capacity. The only way it could become positive is for the

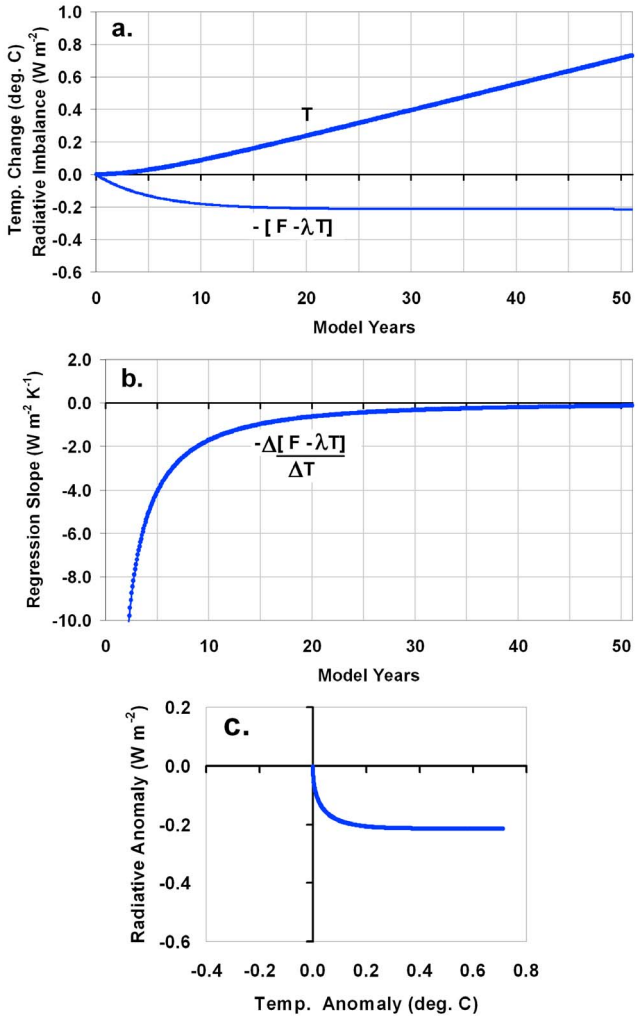

Figure 6. As in Figure 5, but with linearly increasing radiative forcing with time at a rate of 0.4 W m^{-2} per decade.

radiative feedback response to be greater than the radiative forcing, which is physically impossible.

[29] If mistakenly interpreted as the signature of feedback, a negative regression slope would suggest an unstable climate system, with positive feedbacks outweighing the Planck response of 3.3 W m^{-2} K^{-1}. While no one who is knowledgeable would make this mistake for the case of known transient radiative forcing in a model simulation, our point is to introduce the issue of what can happen when diagnosing feedbacks from satellite data if radiative forcing is not accounted for. This simple example of transient radiative forcing demonstrates that the feedback in response to increasing greenhouse gas concentrations cannot be diagnosed from satellite data without somehow correcting for the presence of that forcing. Consistent with FT06's diagnosis of long-term feedbacks in the IPCC AR4 coupled climate models, simply subtracting out the radiative forcing as a function of time from the data in Figure 6 will yield an accurate estimate of the feedback parameter, just as was seen in Figure 5. But without the removal of the transient radiative forcing, the estimate of radiative feedback will be corrupted.

[30] Next we will add another level of realism to the simple model: quasi-random, fluctuations in radiative forcing, as might be expected from nonfeedback fluctuations in low cloud cover. As we will see later, evidence of such internally generated variations in the radiative balance of the climate system is also exhibited by the AR4 coupled climate models.

4.3. Simple Case 3: Random Cloud Variations

[31] Internal radiative forcing from nonfeedback fluctuations in cloud cover could potentially be brought about through circulation-induced changes in tropospheric wind shear, frontal system behavior, precipitation efficiency, trade wind inversion strength, or any other of the myriad processes that can potentially affect cloud formation other than feedback upon temperature. It corresponds to the "*X*" term addressed theoretically by FG06 and is similar to the case analyzed by *Spencer and Braswell* [2008, hereafter SB08].

[32] We use a 7 month low-pass filtered time series of monthly normally distributed random numbers whose long-term average approaches zero for the forcing. The resulting time series of radiative imbalance and temperature are shown in Figure 7a, while the regression slope based upon the accumulated model output is shown in Figure 7b. Despite the feedback parameter value of 2.5 W m^{-2} K^{-1} assumed in the model simulation, regression on all 50 years of model output (Figure 7c) now reveals almost total decorrelation of the data, with the slope of a regression line approaching zero.

[33] But it turns out that the seemingly random distribution of points in Figure 7c once again has structure when one monitors the time evolution of the system with a phase space plot (Figure 7d), as was done with the satellite data in Figures 3 and 4. A looping or spiral pattern emerges in the data, a reflection of the fact that radiative forcing in equation (1) is not proportional to temperature per se, but to the time rate of change of temperature. For instance, it can be shown that if the only source of radiative forcing in equation (1) is a single harmonic function, then the temperature response traces out a circle when the data are plotted in phase space. This is because the forcing and its temperature response are in quadrature, i.e., is separated in phase by 90°. The spiraling or looping character of the system trajectory seen in Figure 7d exists independent of the assumed system heat capacity, feedback strength, or whether the radiative forcing is low-pass filtered random numbers or periodic. Under these different conditions, only the size and the aspect ratio of the loops and spirals change.

[34] Depending upon how the low-pass filtered random radiative forcing evolves over time, slopes based upon only 10 year periods of data (the thin line in Figure 7b) can range from −3 to +6 W m^{-2} K^{-1}. This represents a larger range of slopes than is typically found in satellite data analysis, a problem which will be alleviated with the next level of realism in the model forcing. If the period of record to-date is used in the regression (the thick line in Figure 7b), a more stable regression slope is obtained, but with a fairly persistent low bias approaching 2 W m^{-2} K^{-1}.

[35] Again, the reason why the regression slope does not accurately reflect the feedback specified in the model experiment is that the radiative feedback signal is partly obscured by the time-varying radiative forcing. In fact, if the only source of temperature variability in the system is from time-varying radiative forcing, the feedback is for all practical purposes not observable.

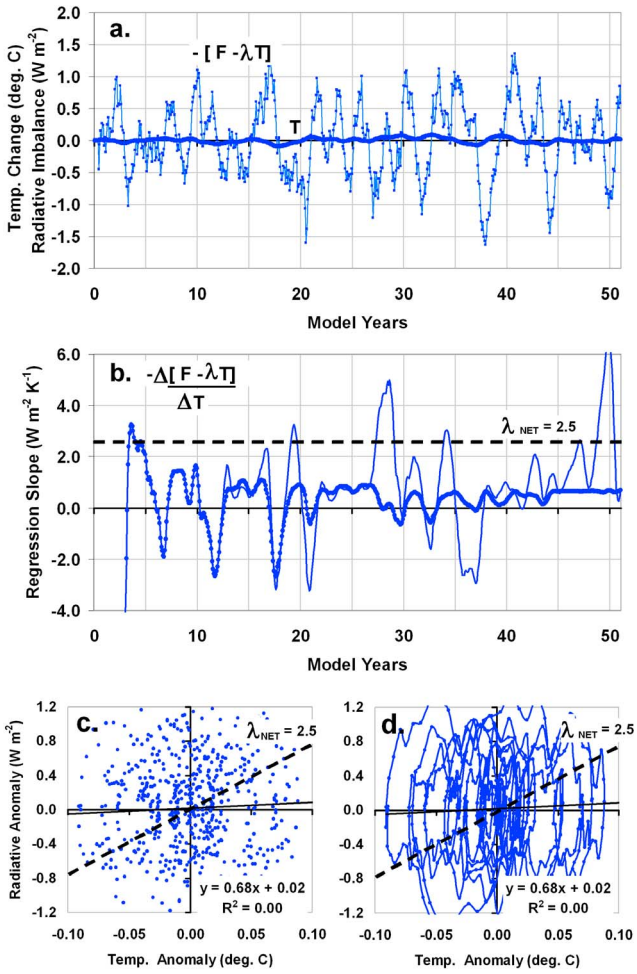

Figure 7. As in Figure 5, but with forcing based upon a time series of low-pass filtered random numbers used for the radiative forcing, the thin line in Figure 7b shows 10 year regression slopes while the thick line shows regressions slopes based upon all model output up to that time and Figure 7d is a phase space plot of the data in Figure 7c. Dashed lines represent the feedback parameter (2.5 W m^{-2} K^{-1}) assumed in the model simulation.

4.4. Importance of Nonradiative Forcing to Feedback Diagnosis

[36] So far, the only behavior we have not seen yet in the simple model that was exhibited by the satellite data is the linear striations shown in Figure 3a. The reason we have not seen such striations is that the model is still missing an important forcing which exists in nature. This additional type of forcing will also explain why the satellite radiative flux variations at high time resolution tend to be negatively correlated with surface temperature, as was seen in Figures 1 and 2.

[37] While the forcing term F in equation (1) has included only radiative components up to this point, nonradiative forcing of temperature also occurs in the climate system, especially on the shorter time scales. Only 1% or 2% variations in the global average rate of convective heat flux from the surface to the atmosphere, which has been estimated to be 100 W m^{-2} [*Kiehl and Trenberth*, 1997], will cause temporary forcings that rival the total estimated anthropogenic radiative forcing to date [*IPCC*, 2007]. Evidence for this process was shown by *Spencer et al*. [2007] in their analysis of a composite of 15 strong tropical intraseasonal oscillations, where strong warming events in the tropical troposphere were accompanied by weak SST cooling. This process was driven by stronger surface winds temporarily enhancing the heat flux from the ocean to the atmosphere.

[38] Note that this type of forcing would not exist if it was the total heat content of the system that was monitored rather than the temperatures of it components. But since feedback is referenced to temperature, our analysis uses temperature, and so we are forced to deal with the complication that the climate system has a variety of temperatures (of the troposphere, upper ocean, and deep ocean) that do not vary in unison. For instance, as can be inferred from the lag correlation plots in Figure 2, tropospheric warming tends to coincide with ocean cooling on short time scales, e.g., weeks or less. Another type of nonradiative forcing would be an SST change caused by a change in the rate of ocean upwelling.

[39] Significantly, nonradiative forcing of temperature is very important to feedback diagnosis because it is the only type of temperature forcing for which the radiative feedback response can be clearly observed in the radiative flux data. This is because, except for the unrealistic special case of constant radiative forcing, only nonradiative forcing of temperature will result in TOA radiative flux variations that are purely due to feedback, with no contamination from radiative forcing. The presence of any time-varying radiative forcing will act to corrupt the diagnosis of feedback, as seen in Figures 6 and 7.

[40] With the addition of nonradiative forcing of temperature, we now have three basic classes of forcing comprising F in equation (1),

$$F(t) = f(t) + N(t) + S(t), \tag{3}$$

where f is any external source of radiative forcing such as anthropogenic greenhouse gas emissions; N is any internally generated nonfeedback source of radiative forcing such as circulation-induced changes in cloud cover; and S is any nonradiative forcing of temperature change such as tropical intraseasonal oscillations in the rate of heat transfer from the ocean to the atmosphere. Including all of these classes of forcing in equation (1), we finally have arrived at the same model formulation used by SB08 to study the potential contamination of radiative feedback estimates by radiative forcing,

$$C_p[dT_{sfc}/dt] = f(t) + N(t) + S(t) - \lambda_{net} T_{sfc}(t), \tag{4}$$

but now we begin to see why the terms in equation (4) were included by SB08. Note that, while the simple model refers to surface temperature, our comparisons to satellite data will be to tropospheric temperature for the reasons discussed in section 3.

[41] If we now run the model represented by equation (4) with various combinations of internal radiative (N) and nonradiative (S) forcings that vary randomly with time, added

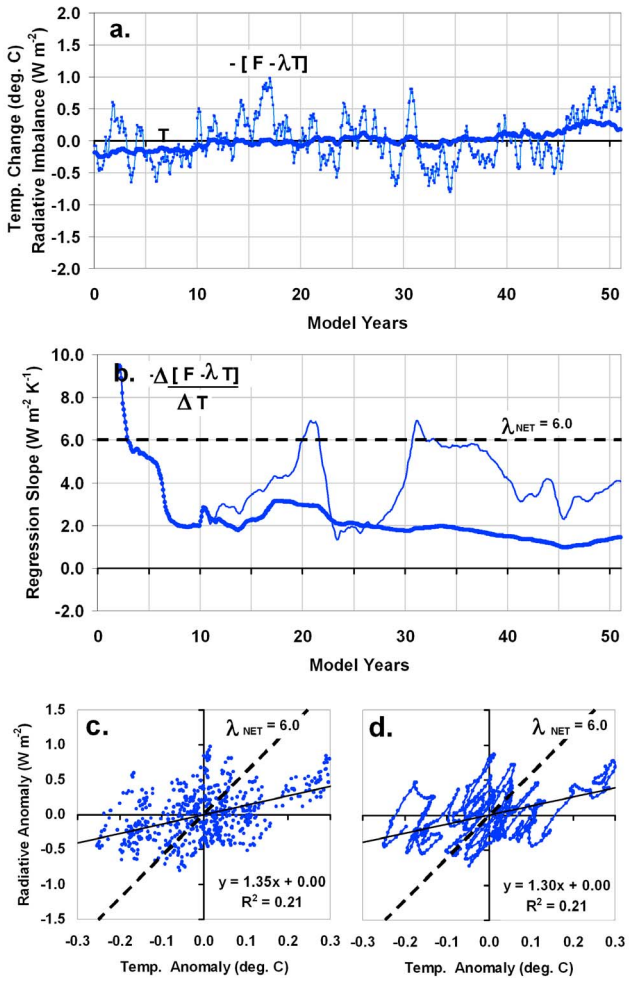

Figure 8. As in Figure 7, but the model is now forced with a combination of transient radiative, low-pass filtered random radiative and low-pass filtered random nonradiative forcings. The specified feedback parameter has been increased to 6 W m^{-2} K^{-1}.

to the transient anthropogenic forcing *f*, we find that a combination of linear and spiral-shaped structures emerge in the phase space plots of temperature versus total radiative flux (see Figure 8). The specified feedback parameter has now been increased to 6 W m^{-2} K^{-1} for this model simulation. Note the linear striations in the data that are approximately parallel to the feedback specified in the model simulation indicated by the dashed line. This potentially explains the linear striations seen in Figure 3a as a reflection of the net feedback operating in the climate system on intraseasonal time scales.

[42] The diagnosed regression slopes in Figure 8b reveal once again that underestimates of the specified feedback almost always occur when there is time-varying radiative forcing present, especially if the whole period of record is used in the regression (thick line). But with nonradiative forcing now present, the variations in the 10 year slopes are not as extreme because feedback now constitutes a larger proportion of the radiative variability. As was shown by SB08, the magnitude of the average low bias in the diagnosed feedback is related to the relative proportions of radiative to nonradiative forcings present in the climate system. Quasi-random radiative forcing without any nonradiative forcing results in a low bias in the diagnosed feedback approaching 100%. This happens around 10 and 25 years into the model simulation in Figure 8b, where a minimum in the diagnosed regression slope occurs. But relatively large levels of nonradiative forcing with little change in radiative forcing will result in feedback diagnosis errors approaching 0%, as seen around 20 and 30 years into the simulation in Figure 8b.

[43] Thus, to the extent that our simple model behaves realistically, we conclude that the accurate diagnosis of radiative feedback from limited satellite data sets becomes a signal-to-noise problem. Nonradiative forcing of temperature provides the feedback signal, while internal radiative forcing produces noise in the form of a decorrelated relationship between radiative flux and temperature. As demonstrated by SB08, the decorrelated component tends to cause a low bias in the diagnosed feedback parameter, although little bias (or even a high bias as seen in Figure 8b) can sometimes result if the period of record being analyzed is short and the proportion of radiative to nonradiative forcing is high.

[44] Next we will examine the behavior of the AR4 coupled climate models to see whether our interpretations based upon the simple climate model are consistent with the behavior exhibited by the more complex climate models.

5. Forcing and Feedback Signatures in the IPCC Climate Models

[45] Now that we have a better understanding of the main categories of processes that can affect the covariations between temperature and radiative flux, we are in a better position to interpret the behavior of the coupled climate models. Our intent is not to diagnose the long-term climate sensitivity in those models, since that has been done fairly accurately by FT06. Instead, we wish to see whether the fully coupled models contain variability that is consistent with our use of and physical interpretations from the simple model.

[46] The coupled model data come from the World Climate Research Programme's (WCRP) Coupled Model Intercomparison Project phase 3 (CMIP3) multimodel data base [*Meehl et al.*, 2007]. We analyzed monthly global anomalies in surface temperature, total LW flux, and total SW flux for the first 50 years of archived transient (1% per year carbon dioxide increase) simulations. Again, the monthly anomalies are computed by subtracting out the multiyear average monthly annual cycles for each variable.

[47] We will show comparisons to surface temperature only since the radiative relationships to tropospheric and surface temperature in the models were very similar. An example of the covariations between LW flux and T_{sfc} anomalies is shown in Figure 9 for the National Center for Atmospheric Research (NCAR) PCM1 model. Running 3 month averages are plotted in Figure 9a, which shows considerable scatter in the data just as we saw from the simple model experiment in Figure 8.

[48] The solid line is a regression fit to the data, while the slope of the dashed line represents the more accurate long-term feedback diagnosed by FT06. In Figure 9b, we have plotted a phase space presentation of the data where 11 month low-pass filtered anomalies are plotted every month and connected by lines.

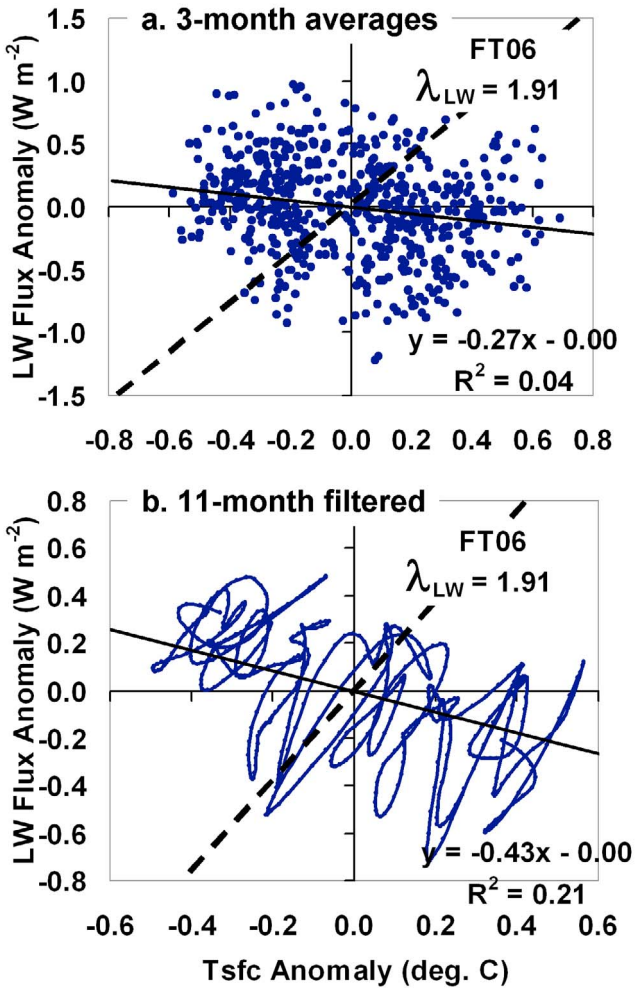

Figure 9. Global average anomalies in the NCAR PCM1 climate model fields of surface temperature versus total top-of-atmosphere LW radiative flux for (a) monthly running 3 month averages and (b) 11 month low-pass filtered averages. The solid lines are regression fits to the data, while the slope of the dashed lines represent the LW feedback parameter diagnosed by FT06.

[49] There are three notable behaviors in the PCM1 model data shown in Figure 9 that can be traced to each of the three classes of forcing included in equation (4). First, the vastly different slopes of the FT06-diagnosed feedback (dashed line) and the regression line slope (solid line) are mostly due to the long-term transient LW radiative forcing imposed upon the model, as was also the case in the simple model example shown in Figure 6. As mentioned previously, this forcing was removed from the model output by FT06 in order to better isolate and diagnose the feedbacks in response to the warming caused by that long-term transient forcing.

[50] Second, the looping or spiral-shaped patterns seen in Figure 9b are similar to behavior observed in the earlier simple model experiment shown in Figure 8 when it was forced by randomly varying radiative and nonradiative forcings. Spiral and looping patterns were the most robust signature we found in the phase space plots of AR4 model output. They were somewhat less apparent in the LW fluxes, but as we will see examples of later, they were clearly apparent in the SW fluxes in all 18 models.

[51] Then third, the linear striations are consistent with the expected signature of feedback upon nonradiative forcing of temperature. As in the simple model plot of Figure 8c, the striations are mixed in with the spiral patterns caused by internal radiative forcing, resulting in a mixing together of these two behaviors. It is presumed that the feedback-induced striations only become clearly apparent when the nonradiative forcing in the model (e.g., fluctuations in ocean-atmosphere heat exchange) is large relative to any fluctuations in internal radiative forcing. We believe that this is the explanation for the striations shown in the monthly global average satellite data of Figure 3a, the slopes of which appear to be around 6 W m^{-2} K^{-1}.

[52] The similarity of the slopes of the linear striations in Figure 9b to the feedback parameter FT06 diagnosed suggests that the short-term and long-term LW feedbacks in the PCM1 model are similar in magnitude. Unfortunately, of the 18 AR4 models we examined, these linear striations in the LW flux component were clearly seen in only four of those models, all shown in Figure 10. In all four the striations are roughly parallel to the long-term feedbacks diagnosed in the models by FT06.

[53] The general lack of striations in the model data is consistent with our observation that there was tighter coupling between surface and tropospheric temperature variations in the AR4 models than we see in the satellite data. This would be consistent with less nonradiative forcing of temperature variations. A more quantitative analysis of any similarities between the striations and the feedbacks diagnosed by FT06 is beyond the scope of this paper. Our goal at this point is simply to establish a better understanding of the ways in which radiative forcing and radiative feedback are expressed in the data.

[54] The corresponding SW relationships for these five models, shown in Figure 11, reveal much better agreement between the regressions slopes computed here and the feedback parameters diagnosed by FT06. The main reason for this agreement is that our SW regressions are substantially the same as those performed by FT06. Because the forcing that was imposed upon the AR4 models in the transient forcing experiments was LW in origin, not SW, there was no long-term SW forcing contaminating the diagnosis of SW feedback response to the LW-induced warming. As a result, our SW regression slopes from the 18 models based upon the 50 year periods of record were highly correlated (r = 0.94) with the SW slopes diagnosed by FT06 for those models.

[55] The AR4 model results for the net (LW + SW) variability, shown in Figure 12, is a combination of the behaviors seen for the LW and SW fluxes separately. Linear striations with a common slope are no longer obvious; we found that none of the 18 models we analyzed showed obvious feedback-induced striations in the net (LW + SW) phase space plots. As alluded to previously, this might be due to the general lack of strong nonradiative forcing events such as tropical intraseasonal oscillations in the coupled climate models [*Lin et al.*, 2006; *Spencer et al.*, 2007]. The regression slopes in Figure 12 are all biased low compared to those diagnosed by FT06, a relationship that existed for all

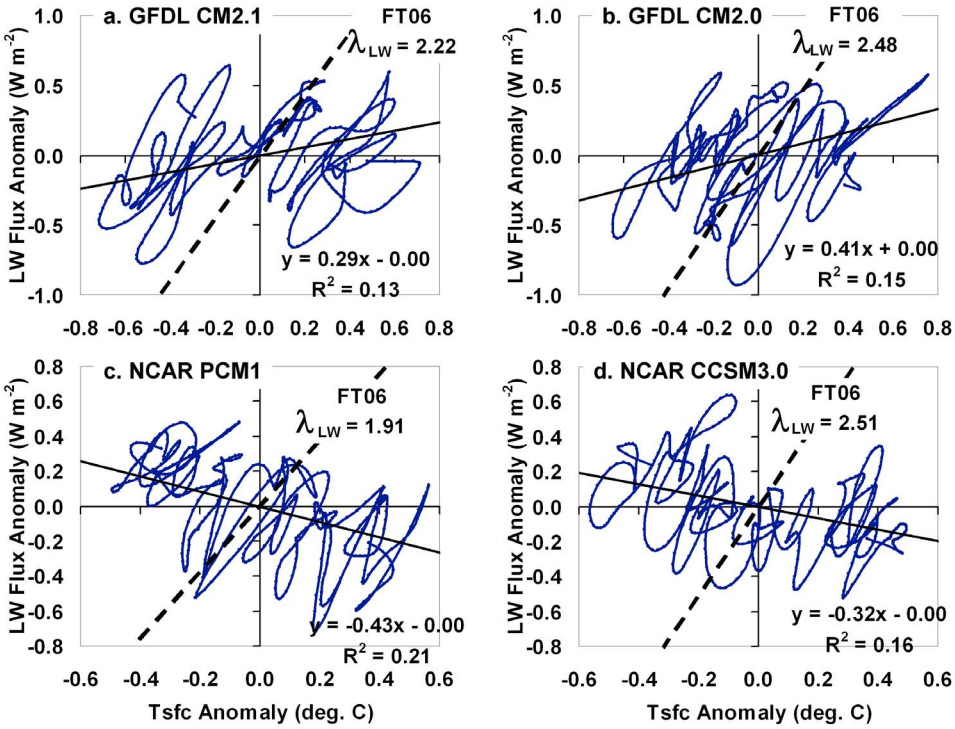

Figure 10. As in Figure 9b, but for the four indicated IPCC AR4 models.

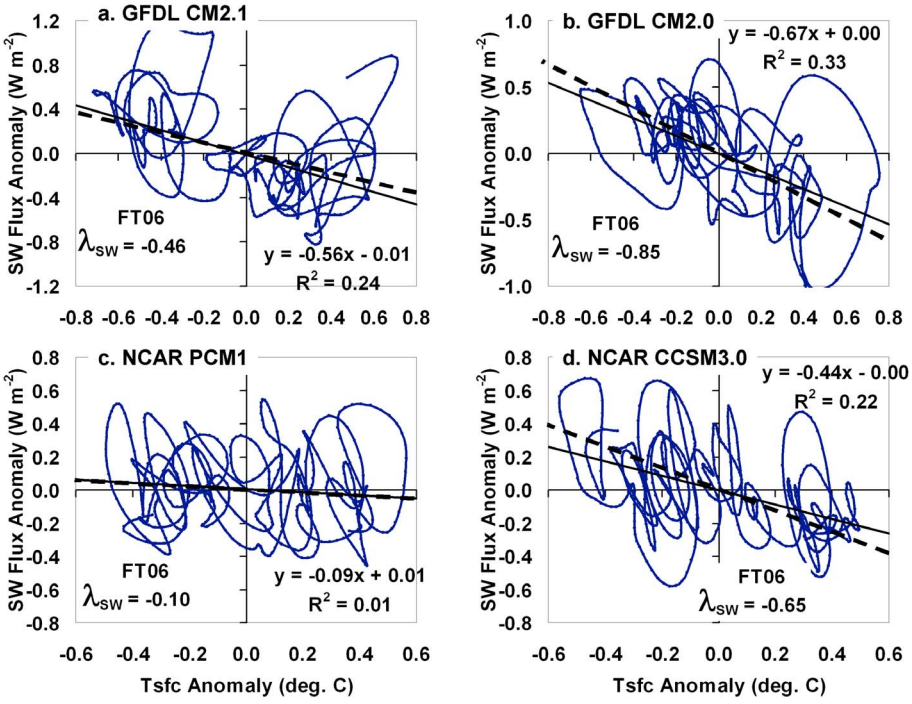

Figure 11. As in Figure 10, except for SW radiative fluxes.

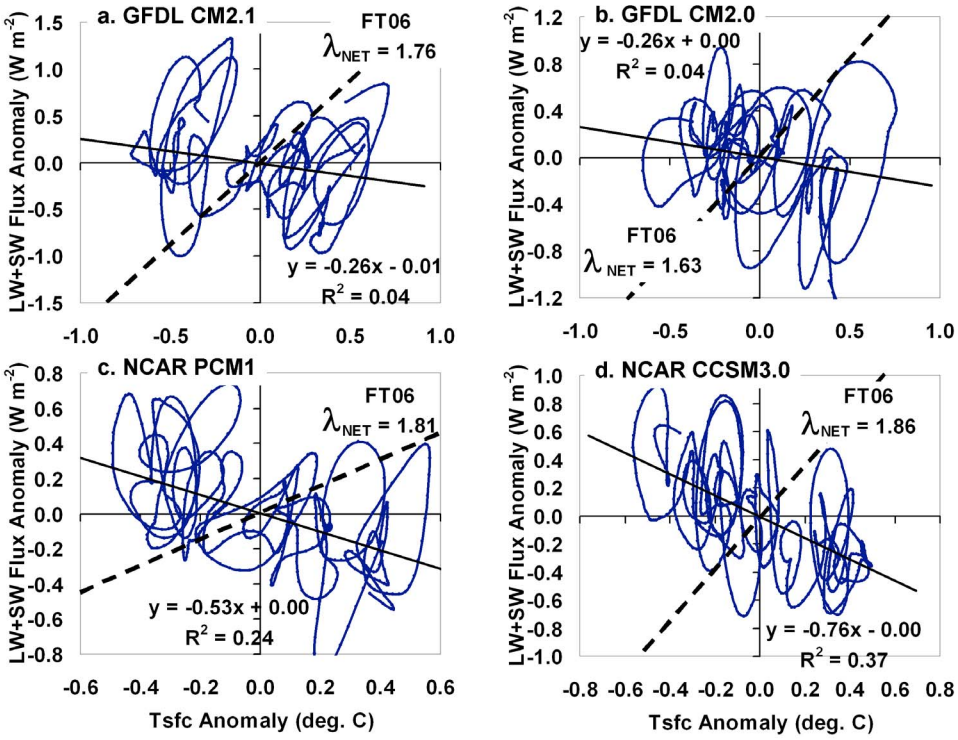

Figure 12. As in Figure 9, but for net (LW + SW) flux.

18 models. Again, this low bias is mostly the result of the long-term LW transient radiative forcing which has not been removed from the model output.

6. Discussion and Conclusions

[56] Previous attempts to diagnose radiative feedback in the climate system from the covariations between TOA radiative flux and temperature have yielded generally low correlations and a wide variety of feedback estimates. The evidence presented here (from satellite, a simple forcing-feedback model, and from coupled climate models) suggests that the dominant source of that decorrelation is the presence of time-varying radiative forcing generated internal to the climate system.

[57] While some might object to the term "internal radiative forcing," it accurately describes both the origin and mechanism of operation within the forcing-feedback construct of climate variability. Any radiative variability that is not due to feedback must be due to forcing. And the alternative term "internal climate variability" does not distinguish between the two different kinds of forcing of temperature change that occur: radiative and nonradiative. The most likely mechanism for this internal radiative forcing is nonfeedback fluctuations in low clouds, although nonfeedback variations in water vapor or high clouds might be a significant component of the decorrelated portion of the LW variations.

[58] It has been demonstrated that radiative feedback in response to unknown levels of time-varying radiative forcing is, for all practical purposes, not observable. This is because the feedback signal is mostly masked by the radiative forcing itself. A simple forcing-feedback climate model, as well as the IPCC AR4 coupled climate models, reveals that quasi-random time-varying internal radiative forcing results in spiral patterns in phase space plots of low-pass filtered temperature and radiative flux variations, patterns which obscure the signature of feedback. Feedback can only be clearly observed in response to nonradiative forcing of temperature, in which case linear striations appear having slopes approximately equal to the feedbacks operating in the models. These striations are believed to only appear during periods when nonradiative forcing is relatively large at the same time that any radiative forcing is relatively constant.

[59] In the AR4 coupled climate models, these striations are obvious in only four models, and then only in the LW, not SW, component. In these four models, the striations lie roughly parallel to the long-term feedbacks previously diagnosed from the models by *Forster and Taylor* [2006]. While supportive of our physical interpretation based upon the simple model experiments, it is premature to claim that the linear striations seen in this handful of AR4 models means that the short-term and long-term feedbacks in the climate system are substantially the same, especially since we could find no obvious linear striations in the SW variations in the AR4 models. The general lack of these feedback signatures in the AR4 models could be due to the relatively weak levels of intraseasonal fluctuations in moist convective activity, for instance the Madden-Julian oscillation [*Lin et al.*, 2006], in the coupled climate models.

[60] Striations in 9 years of global average CERES radiative fluxes from the Terra satellite have a slope around 6 W m^{-2} K^{-1} in net (LW + SW) radiative flux variability. This is similar to the feedbacks diagnosed by *Lindzen and Choi* [2009] from interannual variability in recently recalibrated Earth Radiation Budget Satellite data, as well as that diagnosed for a composite of 15 strong tropical intraseasonal oscillations analyzed by *Spencer et al.* [2007]. Although these

feedback parameter estimates are all similar in magnitude, even if they do represent feedback operating on intraseasonal to interannual time scales, it is not obvious how they relate to long-term climate sensitivity.

[61] Further complicating the diagnosis of feedback from satellite data is the different relationship that radiative flux variations have to surface temperature versus tropospheric temperature on short (intraseasonal) time scales. During nonradiatively forced temperature fluctuations, the signature of feedback is most clearly revealed in response to tropospheric, rather than surface, temperature. Since feedback is traditionally referenced to surface temperature, extra caution must therefore be taken in the physical interpretation of any regression relationships that TOA radiative fluxes have to surface temperature variations.

[62] It also underscores a practical limitation that, since the climate system is never in equilibrium, feedbacks in the climate system cannot be diagnosed from differences between equilibrium climate states. Time-varying radiative and nonradiative forcings are continually occurring, and so radiative feedback parameters will need to be diagnosed in the presence of some level of time-varying radiative forcing, which we have seen usually leads to large errors.

[63] It is clear that the accurate diagnosis of short-term feedbacks (let alone long-term climate sensitivity) from observations of natural fluctuations in the climate system is far from a solved problem. As we have seen, the presence of nonfeedback, internally generated radiative forcing confounds the identification of radiative feedback. Nevertheless, it is hoped that the insights provided here, all explained within the forcing-feedback paradigm of climate variability, will lead to new and more accurate methods of feedback and climate sensitivity diagnosis from satellite observations, as well as better metrics for the testing the climate sensitivity of coupled climate models.

[64] **Acknowledgments.** We acknowledge the modeling groups Program for Climate Model Diagnosis and Intercomparison (PCMDI) and WCRP's Working Group on Coupled Modeling (WGCM) for their roles in making available the WCRP CMIP3 multimodel data set. Support of this data set is provided by the Office of Science, U. S. Department of Energy. This research was supported by NOAA contract NA07OAR4170503 and DOE contract DE-FG02-04ER63841.

References

Aires, F., and W. B. Rossow (2003), Inferring instantaneous, multivariate and nonlinear sensitivities for analysis of feedbacks in a dynamical system: Lorenz model case study, *Q. J. R. Meteorol. Soc.*, *129*, 239–275.

Brohan, P., J. J. Kennedy, I. Harris, S. F. B. Tett, and P. D. Jones (2006), Uncertainty estimates in regional and global observed temperature changes: A new data set from 1850, *J. Geophys. Res.*, *111*, D12106, doi:10.1029/2005JD006548.

Christy, J. R., R. W. Spencer, W. B. Norris, W. D. Braswell, and D. E. Parker (2003), Error estimates of version 5.0 of MSU/AMSU bulk atmospheric temperatures, *J. Atmos. Oceanic Technol.*, *20*, 613–629.

Forster, P. M., and J. M. Gregory (2006), The climate sensitivity and its components diagnosed from Earth Radiation Budget data, *J. Clim.*, *19*, 39–52.

Forster, P. M., and K. E. Taylor (2006), Climate forcings and climate sensitivities diagnosed from coupled climate model integrations, *J. Clim.*, *19*, 6181–6194.

Foster, G., J. D. Annan, G. A. Schmidt, and M. E. Mann (2008), Comment on "Heat capacity, time constant, and sensitivity of Earth's climate system" by S. E. Schwartz, *J. Geophys. Res.*, *113*, D15102, doi:10.1029/2007JD009373.

Gregory, J. M., R. J. Stouffer, S. C. B. Raper, P. A. Stott, and N. A. Rayner (2002), An observationally based estimate of the climate sensitivity, *J. Clim.*, *15*, 3117–3121.

Gregory, J. M., W. J. Ingram, M. A. Palmer, G. S. Jones, P. A. Stott, R. B. Thorpe, J. A. Lowe, T. C Johns, and K. D. Williams (2004), A new method for diagnosing radiative forcing and climate sensitivity, *Geophys. Res. Lett.*, *31*, L03205, doi:10.1029/2003GL018747.

Intergovernmental Panel on Climate Change (IPCC) (2007), *Climate Change 2007: The Physical Science Basis. Contribution of Working Group I to the Fourth Assessment Report of the Intergovernmental Panel on Climate Change*, edited by S. Solomon et al., 996 pp., Cambridge Univ. Press, New York.

Kiehl, J. T., and K. E. Trenberth (1997), Earth's annual global mean energy budget, *Bull. Am. Meteorol. Soc.*, *78*, 197–208.

Kirk-Davidoff, D. B. (2009), On the diagnosis of climate sensitivity using observations of fluctuations, *Atmos. Chem. Phys.*, *9*, 813–822.

Knutti, R., and G. C. Hegerl (2008), The equilibrium sensitivity of the Earth's temperature to radiation changes, *Nat. Geosci.*, *1*, 735–743.

Knutti, R., S. Krahenmann, D. J. Frame, and M. R. Allen (2008), Comment on "Heat capacity, time constant, and sensitivity of Earth's climate system" by S. E. Schwartz, *J. Geophys. Res.*, *113*, D15103, doi:10.1029/2007JD009473.

Lin, J.-L., et al. (2006), Tropical intraseasonal variability in 14 IPCC AR4 climate models: Part I. Convective signals, *J. Clim.*, *19*, 2665–2690.

Lindzen, R. S., and Y.-S. Choi (2009), On the determination of climate feedbacks from ERBE data, *Geophys. Res. Lett.*, *36*, L16705, doi:10.1029/2009GL039628.

Meehl, G. A., C. Covey, T. Delworth, M. Latif, B. McAvaney, J. F. B. Mitchell, R. J. Stouffer, and K. E. Taylor (2007), The WCRP CMIP3 multi-model data set: A new era in climate change research, *Bull. Am. Meteorol. Soc.*, *88*, 1383–1394.

Scafetta, N. (2008), Comment on "Heat capacity, time constant, and sensitivity of Earth's climate system" by S. E. Schwartz, *J. Geophys. Res.*, *113*, D15104, doi:10.1029/2007JD009586.

Schwartz, S. E. J. (2007), Heat capacity, time constant, and sensitivity of Earth's climate system, *J. Geophys. Res.*, *112*, D24S05, doi:10.1029/2007JD008746.

Schwartz, S. E. J. (2008), Reply to comments by G. Foster et al., R. Knutti et al., and N. Scafetta on "Heat capacity, time constant, and sensitivity of Earth's climate system." *J. Geophys. Res.*, *113*, D15105, doi:10.1029/2008JD009872.

Spencer, R. W., and W. D. Braswell (2008), Potential biases in cloud feedback diagnosis: A simple model demonstration, *J. Clim.*, *21*, 5624–5628.

Spencer, R. W., W. D. Braswell, J. R. Christy, and J. Hnilo (2007), Cloud and radiation budget changes associated with tropical intraseasonal oscillations, *Geophys. Res. Lett.*, *34*, L15707, doi:10.1029/2007GL029698.

Stephens, G. L. (2005), Cloud feedbacks in the climate system: A critical review, *J. Clim.*, *18*, 237–273.

Wielicki, B. A., B. R. Barkstrom, E. F. Harrison, R. B. Lee III, G. L. Smith, and J. E. Cooper (1996), Clouds and the Earth's Radiant Energy System (CERES): An Earth Observing System experiment, *Bull. Am. Meteorol. Soc.*, *77*, 853–868.

Wong, T., B. A. Wielicki, R. B. Lee III, G. L. Smith, K. A. Bush, and J. K. Willis (2006), Reexamination of the observed decadal variability in the Earth radiation budget using altitude-corrected ERBE/ERBS nonscanner WFOV data, *J. Clim.*, *19*, 4028–4040.

W. D. Braswell and R. W. Spencer, Earth System Science Center, University of Alabama in Huntsville, Huntsville, AL 35805, USA. (roy.spencer@nsstc.uah.edu)